Quantum Confinement Effects and Electronic Properties of SnO_2 Quantum Wires and Dots

Hui-Xiong Deng, Shu-Shen Li, and Jingbo Li*

State Key Laboratory for Superlattices and Microstructures, Institute of Semiconductors, Chinese Academy of Sciences, P.O. Box 912, Beijing 100083, China

Received: November 20, 2009; Revised Manuscript Received: February 3, 2010

On the basis of the density functional theory (DFT) within local density approximations (LDA) approach, we calculate the band gaps for different size SnO_2 quantum wires (QWs) and quantum dots (QDs). A model is proposed to passivate the surface atoms of SnO_2 QWs and QDs. We find that the band gap increases between QWs and bulk evolve as $\Delta E_g^{wire} = 1.74/d^{1.20}$ as the effective diameter d decreases, while being $\Delta E_g^{dot} = 2.84/d^{1.26}$ for the QDs. Though the $\sim d^{1.2}$ scale is significantly different from $\sim d^2$ of the effective mass result, the ratio of band gap increases between SnO_2 QWs and QDs is 0.609, very close to the effective mass prediction. We also confirm, although the LDA calculations underestimate the band gap, that they give the trend of band gap shift as much as that obtained by the hybrid functional (PBE0) with a rational mixing of 25% Fock exchange and 75% of the conventional Perdew−Burke−Ernzerhof (PBE) exchange functional for the SnO_2 QWs and QDs. The relative deviation of the LDA calculated band gap difference ΔE_g compared with the corresponding PBE0 result is only within 5%. Additionally, it is found the states of valence band maximum (VBM) and conduction band minimum (CBM) of SnO_2 QWs or QDs have a mostly *p*- and *s*-like envelope function symmetry, respectively, from both LDA and PBE0 calculations.

I. Introduction

Semiconductor nanomaterials as the significant foundations for various nanoscale electronic and optoelectronic devices, such as single-electron transistors,[1] single-molecule sensors,[2] and nanowire lasers,[3] have attracted a great deal of attention.[4−13] Nanostructures, such as quantum wires (QWs) and quantum dots (QDs), are of intense scientific and technological interest. Their electronic structures can be tailored by size and shape, leading to many novel physical and chemical properties.[14] Recently, as an ideal material for applications in solar cells,[15] transparent conductors,[16] and gas sensors,[17] SnO_2 QWs or QDs have experimentally been intensively and extensively studied,[18−21] many of which exhibit some unusual and useful properties that have demonstrated significant applications in nanodevices. For example, Xue et al. found that gas sensors based on SnO_2 QWs have short response and recovery time, good selectivity, and low detection limits.[22] However, theoretical studies of electronic properties of SnO_2 QWs or QDs are rarely reported. Theoretically, the electronic properties of QWs or QDs depend not only on their size, geometry, and relaxation but also on the well passivating dangling bonds of surface atoms. For instance, experimentally, large organic molecules are often used to passivate the nanostructure surface. Because of their complexity, this is difficult to implement in realistic calculations. How does one treat the surfaces of SnO_2 QWs or QDs in theory? Apart from this, to achieve a comprehensive guide to experiments, the effects of geometrical shape and size-dependent electronic structures of SnO_2 QWs or QDs are also interesting issues. Therefore, in this work, we perform an extensive first-principles study based on density functional theory (DFT) and detailed analysis of the electronic properties of different size SnO_2 QWs and QDs, respectively. We compare the quantum confinement effects between SnO_2 QWs and QDs. This gives us a good way to understand the effects of dimensionality in quantum confinement systems. In addition, theoretical calculations of QWs or QDs electronic structures usually adopt conventional local density approximations (LDA),[23] but it underestimates the band gap. To test the correctness of the band gap differences between QWs or QDs and bulk from LDA calculations, we further calculate the electronic properties of SnO_2 QWs and QDs using the hybrid functional (PBE0)[24−26] with a rational mixing of 25% Fock exchange and 75% of the conventional Perdew−Burke−Ernzerhof (PBE) exchange functional,[27] which overcomes the LDA band gap error and gives a correct band structure of bulk SnO_2.

II. Computational Details

The electronic properties and total energy calculations are performed utilizing the frozen-core projector-augmented wave (PAW) method[28] within LDA as implemented in VASP codes.[29] Convergence with respect to the plane-wave cutoff energy has been checked. In all calculations, all the atoms are allowed to relax until the quantum mechanical forces acting on them become less than 0.05 eV/Å. The Monkhorst−Pack method[30] is used to sample *k*-point mesh in the Brillouin zone. A $8 \times 8 \times 8$ k-grid is used for the bulk unit cell calculation. While a $1 \times 1 \times 8$ k-grid and only the Γ are used for QWs and QDs, respectively. Usually, the bulk SnO_2 adopts a rutile structure (Figure 1a), and has *P*4_2/*mnm* symmetry. The LDA-optimized parameters are shown in Table 1, in good agreement with the experiments. Next, all constructed QWs and QDs are based on these parameters.

To construct an ideal QW or QD, an important and crucial point is how to deal with the dangling bonds of a surface. Fortunately, theoretically there is a simple and feasible approach of using pseudohydrogen atoms ^ZH, which have a fractional nuclear charge Z and a corresponding fractional electron charge, to passivate the dangling bonds of surface. In our earlier work,[31,32] we have proposed a feasible method to passivate the

* To whom correspondence should be addressed. E-mail: jbli@semi.ac.cn.

10.1021/jp911035z
Published on Web 03/01/2010

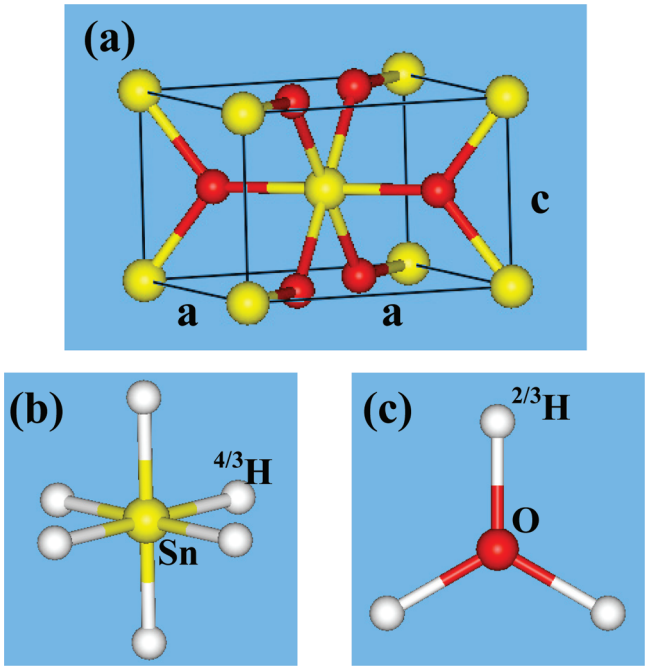

Figure 1. The schematic plots of (a) a primitive unit cell for bulk SnO_2, (b) an octahedral $Sn(^{4/3}H)_6$ structure, and (c) a regular triangular $O(^{2/3}H)_3$ structure. The yellow, red, and white balls represent Sn, O, and pseudohydrogen atoms, respectively. The color scheme is the same for all figures in this paper.

TABLE 1: The LDA Calculated Structural Parameters of Bulk Rutile SnO_2, Compared with the Experimental Results

crystal parameters	LDA	experiment
a	4.727	4.737
c	3.201	3.186
c/*a*	0.677	0.673
u	0.306	0.307

III−V and II−VI QWs and QDs, which obtains some very good results. In this work, we use the following model to passivate the surface atoms of SnO_2 QWs and QDs. In the rutile SnO_2, a Sn atom surrounded by six O atoms has four valence electrons, thus each Sn atom contributes four sixths (2/3) to each band. Because H needs two electrons to have a complete 1*s* shell, we choose the $Z = 2 - 2/3 = 4/3$ pseudohydrogen ($^{4/3}H$) to passivate the Sn dangling bonds. An O atom surrounded by three Sn atoms has six valene electrons, and the stablest state for an O atom has eight electrons forming a closed shell. Therefore, we need $Z = (8 - 6)/3 = 2/3$ pseudohydrogen ($^{2/3}H$) to passivate the O dangling bonds. The next question is how to fix the Sn−$^{4/3}$H and O−$^{2/3}$H bond lengths. We model an octahedral $Sn(^{4/3}H)_6$ and a regular triangular $O(^{2/3}H)_3$, as shown in Figure 1b,c, respectively. Through relaxation optimization, the LDA-calculated Sn−$^{4/3}$H and O−$^{2/3}$H bond lengths are 1.796 and 1.007 Å, respectively. Subsequently, we use these pseudohydrogen atoms along with bond lengths of Sn−$^{4/3}$H and O−$^{2/3}$H to passivate QW and QD surfaces. Basically, we first built a large bulk rutile SnO_2 structure and fixed a Sn atom in the center. Next we chose a sphere with radius *r* (depending on the size of QD), and removed all atoms outside of this sphere. Then, based on the previous molecular dynamics simulations,[33] the surface Sn atoms with more than two dangling bonds and the surface O atoms with more than one dangling bonds were also removed. Finally, we used the $^{4/3}$H and $^{2/3}$H pseudohydrogen atoms to passivate the banding bonds of surface Sn and O, respectively. For the case of QWs, all the building structures

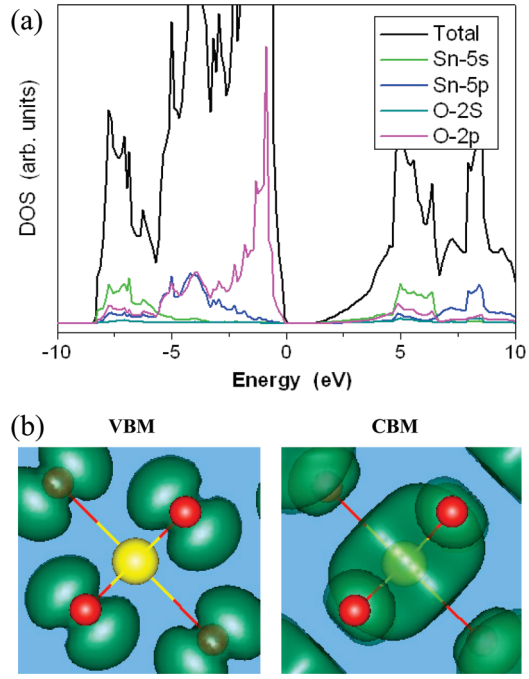

Figure 2. (a) The total and projected DOS for the bulk rutile SnO_2. The VBM is at zero energy. (b) Top view of wave function charge densities of VBM and CBM of the bulk rutile SnO_2.

are periodically extended along the *c* axis, and the (100) crystal face of the rutile structure constitutes the surfaces of QWs. The same passivating scheme is used to terminate the surface Sn and O atoms. In the end, a 10 Å thick layer of vacuum is added in the confined dimensions of all QWs and QDs.

III. Results and Discussion

A. Bulk. Before studying the QWs and QDs, it is necessarily to understand the electronic properties of bulk rutile SnO_2. The rutile SnO_2 has a direct band gap at Γ-point. The LDA calculated the band gap of bulk SnO_2 is 1.10 eV, much smaller than the experimental band gap of 3.6 eV due to the well-known LDA error. In this work, as we only concern band-edge characteristics and the changes of band gap in QWs and QDs, the LDA band gap error will be largely canceled between different systems. In Section E, we will further prove this point using PBE0 calculations that overcome the LDA error. Figure 2a shows the calculated total and projected density of states (DOS) for bulk rutile SnO_2. It is found that the valence band edge of SnO_2 consists mainly of O 2p states, whereas the conduction band edge has a majority of Sn 5s and a minority of O 2p characters. As also can be seen from the wave function charge densities of valence band maximum (VBM) and conduction band minimum (CBM) of rutile bulk SnO_2 in Figure 2b, the VBM totally localizes on the O site, and has p-state character, while the CBM is mostly localized on Sn, and a bit on the O sites.

B. Quantum Wires. We calculated four different size nanowires: $Sn_5O_{10}(^{4/3}H)_6(^{2/3}H)_6$, $Sn_{13}O_{26}(^{4/3}H)_{10}(^{2/3}H)_{10}$, $Sn_{25}O_{50}(^{4/3}H)_{14}(^{2/3}H)_{14}$, and $Sn_{41}O_{82}(^{4/3}H)_{18}(^{2/3}H)_{18}$. All QWs are chemically stoichiometrical. The corresponding ratios of length (along the *c* axis) to the effective diameter are 0.43, 0.26, 0.19 and 0.15, respectively. Here, the effective diameter of QWs is defined in terms of the total number (N_{wire}) of Sn and O atoms (i.e., not counting the surface pseudohydrogen atoms) in a wire as $d = (N_{wire}/6a^2)^{1/2}$, where *a* is the LDA-optimized lattice parameter (Table 1). The LDA-calculated band gaps for all different size QWs are listed in Table 2. It is clearly found the band gaps of

TABLE 2: Summary of Computational Details, As Well As the Calculated Band Gaps and ΔE_g of Different Size SnO_2 QWs and QDs

	number of atoms							
nanostructures	total	Sn	O	$^{4/3}$H	$^{2/3}$H	diameter (nm)	E_g (eV)	$\Delta E_g = E_g - E_g^{bulk}$ (eV)
wires	27	5	10	6	6	0.75	3.53	2.43
	59	13	26	10	10	1.21	2.55	1.45
	103	25	50	14	14	1.67	2.02	0.92
	159	41	82	18	18	2.14	1.73	0.63
dots	86	14	22	34	16	0.94	4.14	3.04
	159	29	60	32	38	1.27	3.29	2.19
	347	69	140	66	72	1.68	2.51	1.41
	453	99	196	82	76	1.89	2.36	1.26

QWs increase as the effective diameter of QWs decreases. Compared to a bulk band gap of 1.10 eV, there exists a remarkable quantum confinement effect in the QWs. The band gap differences between QWs and bulk can be fitted using the expression $\Delta E_g^{wire} = E_g^{wire} - E_g^{bulk} = \beta_{wire}/d^{\alpha_{wire}}$. The analytic fitting results of QWs are shown in Figure 3. We obtain $\alpha_{wire} = 1.20$ and $\beta_{wire} = 1.74$, in a agreement with the experiment.[34] For example, in terms of these fitting parameters, we calculated the band gap difference from bulk for QW is 0.76 eV when the effective diameter $d = 2.0$ nm, close to the experimental value of about 0.6 eV in ref 34. According to the previous first-principles calculations,[31] the values of α_{wire} are about 1.0 for III−V QWs, and 1.53 for the Si QWs. While values of β_{wire} are between 1.5 and 2.5 for II−VI and III−V QWs. From these points of view, our results have a fair amount of creditability and correctness.

C. Quantum Dots. In this subsection, we calculated four QDs: $Sn_{14}O_{22}(^{4/3}H)_{34}(^{2/3}H)_{16}$, $Sn_{29}O_{60}(^{4/3}H)_{32}(^{2/3}H)_{38}$, $Sn_{69}O_{140}(^{4/3}H)_{66}(^{2/3}H)_{72}$, and $Sn_{99}O_{196}(^{4/3}H)_{82}(^{2/3}H)_{76}$. Excluding the pseudohydrogen atoms, the total numbers (N_{dot}) of Sn and O atoms are 36, 89, 209 and 295, respectively. We estimate that the corresponding effective diameters are 0.94, 1.27, 1.68, and 1.89 nm (Table 2) in terms of the expression of $d = (a^2cN_{dot}/\pi)^{1/3}$, where a and c are the LDA optimized lattice constants of rutile SnO_2. The LDA calculated the band gaps of different size QDs are shown in Table 2. As expected, as the size decreases, the gap of QD becomes larger and larger as a result of the quantum confinement effect. Similarly, we use the expression $\Delta E_g^{dot} = \beta_{dot}/d^{\alpha_{dot}}$ to fit the band gap increases between QDs and bulk as the effective diameter d decreases (Figure 3). As a result, we get $\alpha_{dot} = 1.26$ and $\beta_{dot} = 2.84$. In the previous first-principles studies,[31] it is found that, for the III−V and II−VI QDs, the values of α_{dot} are between 1.0 and 1.3, and β_{dot} values are slightly larger than 3.0.

Next, It is significant to compare quantum confinement effects between the SnO_2 QWs and QDs. A effective way of comparing quantum confinement effects is the ratio of band gap shifts ($\Delta E_g^{wire}/\Delta E_g^{dot}$) between QWs and QDs. In terms of a simple effective-mass approximation (EMA) model,[35−37] the band gap shifts of QDs and QWs from the bulk value are $\Delta E_g = (2\hbar^2\mathcal{Z}^2)/(m^*d^2)$, where, $1/(m^*) = 1/(m_e^*) + 1/(m_h^*)$ (m_e^* and m_h^* are electron and hole effective-masses, respectively). For spherical QDs, $\mathcal{Z}^{dot} = \pi$ is the zero point of the spherical Bessel function and $\mathcal{Z}^{wire} = 2.4048$ is the zero point of the cylindrical Bessel function for cylindrical QWs. Because QWs and QDs have the same decreasing scale ($\sim d^{-2}$) as the effective diameter increases for the EMA model, we can simply calculate the ratio $\Delta E_g^{wire}/\Delta E_g^{dot} = (\mathcal{Z}^{wire})^2/(\mathcal{Z}^{dot})^2 = 0.586$.[31] However, in our fitting ΔE_g expressions of the SnO_2 QWs and QDs, they do not have the same scale, and we cannot directly obtain the $\Delta E_g^{wire}/\Delta E_g^{dot}$, which depends on d. Therefore, we assume that α_{dot} is the same as α_{wire}, and use the α_{dot} to fit the ΔE_g^{wire}. This gives us a new β'_{wire}. As a result, the $\Delta E_g^{wire}/\Delta E_g^{dot}$ ratio will just be the ratio of $\beta'_{wire}/\beta_{dot}$. Thus, we obtain this ratio as 0.609, very close to the simple effective mass prediction. Additionally, we also find that the difference for α between QW and QD is very small. The

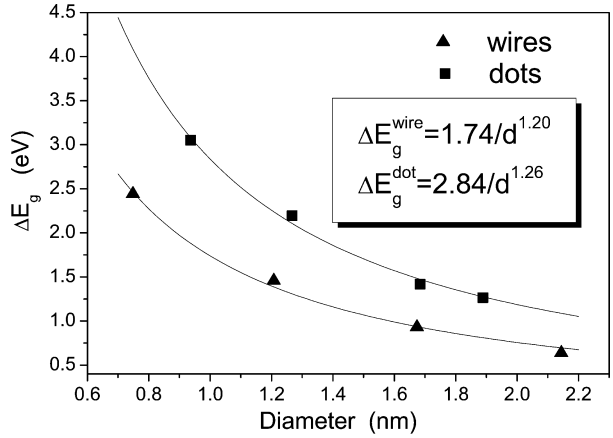

Figure 3. The calculated band gaps of different size SnO_2 QWs and QDs. The lines are the fitted curves: $\Delta E_g^{wire} = 1.74/d^{1.20}$ for the QWs, and $\Delta E_g^{dot} = 2.84/d^{1.26}$ for the QDs.

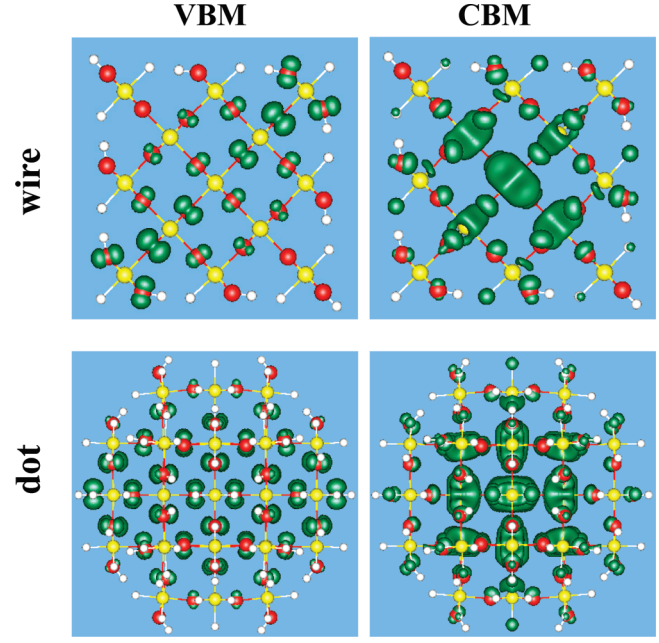

Figure 4. The wave function square contour plots of VBM and CBM of the SnO_2 QW and QD from LDA calculations. The diameters of the QW and QD are 1.21 and 1.89 nm, respectively. All the plots are views from the (001) direction.

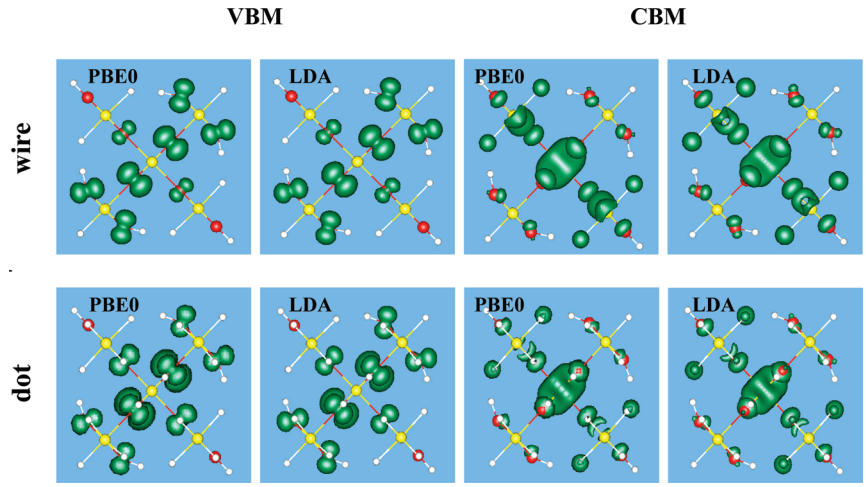

Figure 5. (color online) Comparisons of the wave function square contour plots of VBM and CBM from LDA and PBE0 calculations, respectively, for the QW ($Sn_5O_{10}(^{4/3}H)_6(^{2/3}H)_6$) and QD($Sn_{14}O_{22}(^{4/3}H)_{34}(^{2/3}H)_{16}$). All the plots are the views from (001) direction.

ratio of $(\alpha_{dot} - \alpha_{wire})/\alpha_{dot}$ is only within 5%, in a good agreement with the prediction of ref 31.

D. Wave Function Characteristics of VBM and CBM. As we known, the wave function characteristics of VBM and CBM of the QWs or QDs have profound effects on their potential device applications. So, in order to make the natures of these bands more clear, we have calculated the wave function squares of VBM and CBM for fully passivated QWS and QDs. Figure 4 shows the wave function squares of a selected QW and QD from the view along the (001) direction. We find: (i) the VBM state of QWs and QDs has a predominantly *p*-like envelope function symmetry, and the CBM has a mostly *s*-like envelope function symmetry. This can be simply accounted for by the fact that the VBM envelope has a zero wave function amplitude at the origin (the QW or QD center in Figure 4), which can be represented by spherical Bessel function $J_{L=1}(\xi r)$, while CBM envelope has the maximum wave function amplitude at the origin and can be represented by $J_{L=0}(\xi r)$. Consequently, they have *p*- and *s*-like envelope characteristics, respectively. (ii) The wave functions of CBM and VBM are mostly distributed in the interior of QW or QD, which indicates that the surface passivating manner is very effective.

E. Comparison between LDA and PBE0 Calculations. To overcome the well-known LDA error and further verify the correctness of band gap differences ΔE_g between SnO_2 QWs or QDs and bulk from LDA calculations, we have calculated the accurate band gap of a small SnO_2 QW and QD with the PBE0 method based on VASP codes with version 5.2.[29] The PBE0 gives the band gap of 3.70 eV of bulk rutile SnO_2, in a agreement with experimental value. The PBE0 calculated band gap differences of the QW with atom configuration Sn_5 O_{10} $(^{4/3}H)_6$ $(^{2/3}H)_6$ and QD with atom configuration Sn_{14} O_{22} $(^{4/3}H)_{34}$ $(^{2/3}H)_{16}$ from the bulk are 2.35 and 2.92 eV, respectively (Table 3). So, the relative deviation of band gap differences from LDA calculations can be measured by comparing to the PBE0 results as follows: $\sigma(d) = (\Delta E_{g,\,LDA}(d) - \Delta E_{g,\,PBE0}(d))/\Delta E_{g,\,PBE0}(d)$. We get the values $\sigma(d)$ of 3.4% for the QW and 4.1% for the QD. As expected, although the LDA calculations underestimate the band gap, they give the trend of band gap shift as much as PBE0 calculations for the SnO_2 QWs and QDs. Due to the PBE0 calculations expend too much computing cost, we simply select a very small QW and QD to perform PBE0 calculations. It is necessary to point out that, as the effective diameter *d* of QWs or QDs increases, the deviation $\sigma(d)$ will reduce because of the energy difference $\Delta E(d \rightarrow \infty) = Eg(d \rightarrow \infty) - E_g^{bulk} = 0$ from whether PBE0 or LDA calculations. Figure 5 depicts comparisons of the wave function square contour of VBM and CBM of the SnO_2 QW and QD from PBE0 and LDA calculations. We can see that the VBM or CBM state of the QW or QD has the same envelope function symmetry between PBE0 and LDA calculations. This reflects the LDA calculated characteristics of band edges of QWs and QDs are reasonable.

TABLE 3: Comparisons of Band-Gap Shift Calculated from PBE0 and LDA Methods, Respectively, for a Small SnO_2 QW ($Sn_5O_{10}(^{4/3}H)_6(^{2/3}H)_6$) and QD ($Sn_{14}O_{22}(^{4/3}H)_{34}(^{2/3}H)_{16}$)

method	E_g^{bulk}	E_g^{wire}	ΔE_g^{wire}	E_g^{dot}	ΔE_g^{dot}
PBE0	3.70	6.05	2.35	6.62	2.92
LDA	1.10	3.53	2.43	4.14	3.04

IV. Summary

In summary, using the DFT within LDA, we studied the electronic properties of different size SnO_2 QWs and QDs. Through calculations of band gaps of the different size QWs and QDs, we find, as the size changes, the band gap evolves as $E_g(\text{wire}) = E_g(\text{bulk}) + 1.74/d^{1.20}$ for the QWs, while $E_g(dot) = E_g(bulk) + 2.84/d^{1.26}$ for the QDs, basically consistent with the prediction of the previous first-principle studies. We also confirm LDA calculations give the trend of band gap shift as much as PBE0 for the QWs and QDs. In additional, based on both the PBE0 and LDA calculations, we find that the VBM and CBM of SnO_2 QWs and QDs have a mostly *p*- and *s*-like envelope function symmetry, respectively.

Acknowledgment. J.L. gratefully acknowledges financial support from the "One-Hundred Talent Plan" of the Chinese Academy of Sciences and National Science Fund for Distinguished Young Scholar (Grant No. 60925016). This work is supported by the National High Technology Research and Development program of China under Contract No. 2009AA034101, the National Basic Research Program of China (973 Program) Grant No. G2009CB929300, and the National Natural Science foundation of China under Grant Nos. 60521001 and 6077061.

References and Notes

(1) Akiyama, T.; Wada, O.; Kuwatsuka, H.; Simoyama, T.; Nakata, Y.; Mukai, K.; Sugawara, M.; Ishikawa, H. *Appl. Phys. Lett.* **2000**, *77*, 1753.

(2) Duan, X.; Huang, Y.; Agarval, R.; Lieber, C. M. *Nature* **2003**, *421*, 241.

(3) Wang, W. U.; Chen, C.; Lin, K. H.; Fang, Y.; Lieber, C. M. *Proc. Natl. Acad. Sci. U.S.A.* **2005**, *102*, 3208.
(4) Huang, M. H.; Mao, S.; Feick, H.; Yan, H. Q.; Wu, Y. Y.; Kind, H.; Weber, E.; Russo, R.; Yang, P. D. *Science* **2001**, *292*, 1897.
(5) Milliron, D. J.; Hughes, S. M.; Cui, Y.; Manna, L.; Li, J.; Wang, L. W.; Alivisatos, A. P. *Nature* **2004**, *430*, 190.
(6) Yu, H.; Li, J.; Loomis, R. A.; Wang, L. W.; Buhro, W. E. *Nat. Mater.* **2003**, *2*, 517.
(7) Kilina, S. V.; Craig, C. F.; Kilin, D. S.; Prezhdo, O. V. *J. Phys. Chem. C* **2007**, *111*, 4871.
(8) Isborn, C. M.; Kilina, S. V.; Li, X. S.; Prezhdo, O. V. *J. Phys. Chem. C* **2008**, *112*, 18291.
(9) Isborn, C. M.; Prezhdo, O. V. *J. Phys. Chem. C* **2009**, *113*, 12617.
(10) Sashchiuk, A.; Langof, L.; Chaim, R.; Lifshitz, E. *J. Cryst. Growth* **2002**, *240*, 431.
(11) Li, S. Q.; Liang, Y. X.; Wang, T. H. *Appl. Phys. Lett.* **2005**, *87*, 143104.
(12) Moreels, I.; Lambert, K.; Muynck, D. D.; Vanhaecke, F.; Poelman, D.; Martins, J. C.; Allan, G.; Hens, Z. *Chem. Mater.* **2007**, *19*, 6101.
(13) Chen, Z. W.; Lai, J. K. L.; Shek, C. H. *Appl. Phys. Lett.* **2006**, *88*, 033115.
(14) (a) Li, J.; Wang, L. W. *Nano Lett.* **2003**, *3*, 101. (b) Li, J.; Wang, L. W. *Nano Lett.* **2003**, *3*, 1357. (c) Li, J.; Wang, L. W. *Nano Lett.* **2004**, *4*, 29.
(15) Bachmann, K. J.; Schreiber, H., Jr., W. R. S.; Schmidt, P. H.; Thiel, F. A.; Spencer, E. G.; Pasteur, G.; Feldmann, W. L.; SreeHarsha, K. *J. Appl. Phys.* **1979**, *50*, 3441.
(16) Kilic, C.; Zunger, A. *Phys. Rev. Lett.* **2002**, *88*, 095−501.
(17) Lee, D. S.; Rue, G. H.; Huh, J. S.; Choi, S. D.; Lee, D. D. *Sens. Actuators B* **2001**, *77*, 90.
(18) Chiodini, N.; Paleari, A.; DiMartino, D.; Spinolo, G. *Appl. Phys. Lett.* **2002**, *81*, 1702.
(19) Lee, E. J. H.; Ribeiro, C.; Giraldi, T. R.; Longo, E.; Leite, E. R.; Varela, J. A. *Appl. Phys. Lett.* **2004**, *84*, 1745.
(20) Xue, X. Y.; Chen, Y. J.; Wang, Y. G.; Wang, T. H. *Appl. Phys. Lett.* **2005**, *86*, 233101. Xue, X. Y.; Chen, Y. J.; Li, Q. H.; Wang, C.; Wang, Y. G.; Wang, T. H. *Appl. Phys. Lett.* **2006**, *88*, 182102.
(21) Li, L.; Zong, F.; Cui, X.; Ma, H.; Wu, X.; Zhang, Q.; Wang, Y.; Yang, F.; Zhao, J. *Mater. Lett.* **2007**, *61*, 4152.
(22) Xue, X. Y.; Chen, Y. J.; Liu, Y. G.; Shi, S. L.; Wang, Y. G.; Wang, T. H. *Appl. Phys. Lett.* **2006**, *88*, 201907.
(23) Kohn, W.; Sham, L. J. *Phys. Rev. B* **1965**, *140*, A1133.
(24) Perdew, J. P.; Ernzerhof, M.; Burke, K. *J. Chem. Phys.* **1996**, *105*, 9982.
(25) Adamo, C.; Barone, V. *J. Chem. Phys.* **1999**, *110*, 6158.
(26) Paier, J.; Marsman, M.; Hummer, K.; Kresse, G.; Gerber, I. C.; Angyan, J. G. *J. Chem. Phys.* **2006**, *124*, 154709.
(27) Perdew, J. P.; Burke, K.; Ernzerhof, M. *Phys. Rev. Lett.* **1996**, *77*, 3865.
(28) Blöchl, P. E. *Phys. Rev. B* **1994**, *50*, 17953. Kresse, G.; Joubert, J. *Phys. Rev. B* **1999**, *59*, 1758.
(29) (a) Kresse, G.; Hafner, J. *Phys. Rev. B* **1993**, *47*, R558. (b) Kresse, G.; Hafner, J. *Phys. Rev. B* **1993**, *48*, 13115.
(30) Monkhorst, H. J.; Pack, J. D. *Phys. Rev. B* **1976**, *13*, 5188.
(31) (a) Li, J.; Wang, L. W. *Chem. Mater.* **2004**, *16*, 4012. (b) Li, J.; Wang, L. W. *Phys. Rev. B* **2005**, *72*, 125325.
(32) (a) Peng, H.; Li, J.; Li, S.-S.; Xia, J.-B. *J. Phys. Chem. C* **2008**, *112*, 13964. (b) Peng, H.; Li, J. *J. Phys. Chem. C* **2008**, *112*, 20241.
(33) Naicker, P. K.; Cummings, P. T.; Zhang, H.; Banfield, J. F. *J. Phys. Chem. B* **2005**, *109*, 15243.
(34) Xu, X.; Zhuang, J.; Wang, X. *J. Am. Chem. Soc.* **2008**, *130*, 12527.
(35) Li, J.; Xia, J. B. *Phys. Rev. B* **2000**, *61*, 15880.
(36) Li, J.; Xia, J. B. *Phys. Rev. B* **2000**, *62*, 12613.
(37) Zheng, W. H.; Xia, J. B.; Cheah, K. W. *J. Phys.: Condens. Matter* **1997**, *9*, 5105.

JP911035Z